

Influence of dendrite arm spacing on the thermal conductivity of an aluminum-silicon casting alloy

C. Vázquez-López

Departamento de Física, Centro de Investigación y de Estudios Avanzados del IPN, A. P. 14-740, México, 07000, D.F., Mexico

A. Calderón and M.E. Rodríguez

Centro de Investigación en Ciencia Aplicada y Tecnología Avanzada del IPN, Calzada Legaria No. 694, Col. Irrigación, México 11500, D.F. Mexico

E. Velasco and S. Cano

Corporativo Nemak, S. A. de C. V., A. P. A-100, Monterrey, 66000, N.L. Mexico

R. Colás

Facultad de Ingeniería Mecánica y Eléctrica, Universidad Autónoma de Nuevo León, A. P. 149-F, Cd. Universitaria, San Nicolás de los Garza, 66451, N.L. Mexico

S. Valtierra

Corporativo Nemak, S. A. de C. V., A. P. A-100, Monterrey, 66000, N.L. Mexico

(Received 27 May 1999; accepted 7 October 1999)

The photoacoustic technique and the thermal relaxation method were used to determine the thermal conductivity of some representative samples obtained from an aluminum-silicon casting alloy A319. This material was solidified with an imposed unidirectional thermal gradient to obtain samples with different microstructures characterized by the secondary dendrite arm spacing, which increases as the solidification rate decreases. It was found that the thermal conductivity of the alloy decreases with an increase in the secondary dendrite arm spacing and a decrease in the integral dendrite perimeter.

I. INTRODUCTION

The importance of simple thermal diffusivity measurements is crucial in the use of several industrial alloys, in particular those which are subjected to thermal cycling, such as aluminum alloys employed in the manufacture of automotive engines, since power dissipation is an important mechanism in engine performance.¹

The microstructure which is developed in a casting depends on its solidification rate.^{2,3} In the case of the widely used hypoeutectic aluminum silicon alloys, the typical microstructure is composed of aluminum dendrites and a dispersion of the eutectic when made from aluminum and nearly pure silicon.^{2,3} The secondary dendrite arm spacing (DAS) was found to be reduced as the solidification rate increased,^{3,4} whereas the shape and distribution of eutectic silicon is affected by a series of parameters such as solidification rate and chemical composition.⁵⁻⁷

It is a well-known fact that the physical and mechanical properties of a material depend on its microstructure,^{5,6,8,9} but the relationship between the thermophysical properties and microstructure is perhaps less studied, although some reports^{9,10} indicate that the electrical conductivity depends on the microstructure.

The experimental methods commonly employed to determine the thermal diffusivity in materials are of three different types, depending on whether the measured heat flow is stationary, (conventional method¹¹) transient or periodic. The American Society for Testing Materials considers as standard a version of the transient technique, the laser flash method,¹² to determine the thermal diffusivity. The periodic method was introduced in 1863 by Ångström,¹³ and involves heating periodically one end of a rod-shaped sample and measuring the resulting temperature oscillations at another point of the rod. The phase lag between the thermal oscillations at any two points gives a precise determination of the thermal diffusivity. Another method, applied in this work, which is based on the photoacoustic (PA) technique¹⁴ has been employed extensively¹⁵⁻¹⁸ and has the advantage of requiring small quantities of the material to be analyzed, permitting the determination of the thermal diffusivity in localized regions of the material.

The aim of this work is to determine the possible correlation between the thermophysical properties and the position-dependent microstructure of a commercial aluminum casting alloy of the type A319.

II. EXPERIMENTAL PROCEDURE

The experimental alloy was obtained from a computer-controlled instrumented rig, which consisted of a 51-mm-thick steel plate and a mast in which a given number (normally eight) of type K (chromel-alumel) thermocouples are localized at different heights. The thermocouples were connected, during testing, to a solid-state device used to convert the electromotive force, generated by the couple, into a linear scale ranging from 0 to 5 V. The output from these appliances was then applied to an analog-digital board installed in a PC-compatible computer.

Figure 1 shows a representation indicating the positions at which the thermocouples were inserted. Cooling of the bottom surface of the steel was accelerated by water. The aluminum alloy was poured into an ingot mould (made of recrystallized alumina) of 150-mm diameter and 300-mm height, which was covered with a ceramic fibre blanket in order to assure unidirectional solidification. The thermocouples were located in this particular experiment at the ingot-steel plate interface (which will be called zero distance), and at 1, 2, 4, 8, and 12 cm from the interface. Small samples were cut from the ingot from positions close to those of the thermocouples in order to correlate the thermal evolution during solidification with the microstructure and thermophysical properties. The samples were approximately 300- μm -thick, and had an area of $0.5 \times 0.5 \text{ cm}^2$. The chemical

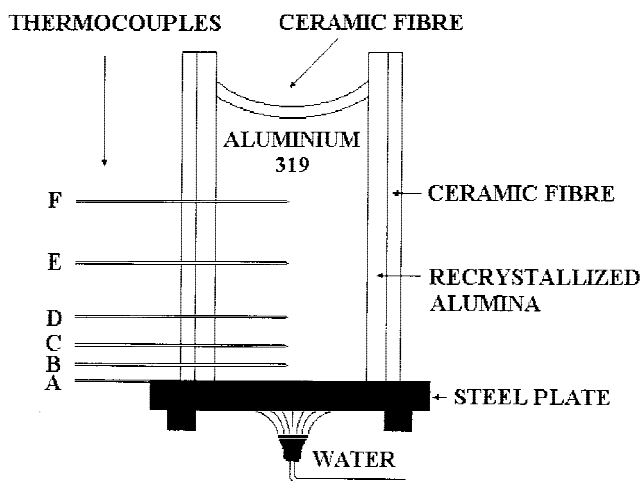


FIG. 1. Experimental casting setup. The thermocouples are used to monitor the position-dependent solidification process.

TABLE I. Chemical analysis (wt.%) of different heights of the cast ingot (Fig. 1).

Sample	Si	Cu	Fe	Mn	Mg	Zn	Ti	Sr	Al
A	7.05	3.34	0.56	0.32	0.29	0.67	0.14	0.01	87.61
B	7.75	3.55	0.63	0.35	0.31	0.70	0.12	0.01	86.58
C	7.70	3.50	0.67	0.39	0.30	0.70	0.12	0.01	86.61
D	7.56	3.14	0.77	0.46	0.28	0.67	0.14	0.01	86.97
E	7.73	3.27	0.67	0.40	0.28	0.67	0.14	0.01	86.83
F	7.82	3.38	0.59	0.31	0.31	0.69	0.11	0.01	86.77

composition of the alloy was determined by optical emission spectroscopy (spark) as a function of the position. The averaged values are reported in Table I. The microstructure of the samples was determined with a Nikon Epiphot TME metallographic microscope (Japan), once the dendrites were revealed with an aqueous solution of 0.05% HF. Measurements of the secondary DAS and of the total length of the dendrite coastlines, which will be called the “perimeter” were conducted along different radial directions, normal to the solidification direction. The average was obtained from at least 150 branches.

The thermal diffusivity was determined by the PA technique employing the open photoacoustic cell (OPC) configuration.¹⁴ The schematic experimental array is shown in Fig. 2. In this arrangement the sample is fixed with vacuum grease at the top of a commercial electret microphone in order to detect the PA signal. The front air chamber adjacent to the metallized face of the microphone diaphragm plays the role of the PA chamber. The experimental setup consists of an 80 mW Ar laser, whose monochromatic light beam (488 nm line) was mechanically modulated with a variable speed mechanical chopper (SRS-model 540) and uniformly focused on the sample. An interference filter was used in order to avoid the UV plasma components of the laser. Part of the incident light is converted into heat that propagates through the sample. Then it induces pressure fluctuations in the PA cell. A lock-in amplifier (SRS-model 850, Sunnysvale, CA) connected to a personal computer through an IEEE-488 card is used to analyze the output voltage and the phase lag from the microphone, as a function of the modulation frequency.

According to the theory of the OPC configuration for opaque solids, the influence of the thermal diffusivity process on the magnitude and the phase lag of the microphone output are given, respectively, by

$$A = \frac{C_o f^{-1}}{\sqrt{\cosh(2aL) - \cos(2aL)}} \quad \text{and} \quad (1)$$

$$\Delta\phi = -\text{atan} \left[\frac{\tan(aL)}{\tanh(aL)} \right] - \pi/2 \quad (2)$$

In these expressions, C_o is a factor that depends on the geometrical and dielectric properties of the microphone, $a = \sqrt{\pi f/\alpha}$ is the thermal diffusion coefficient, f is the

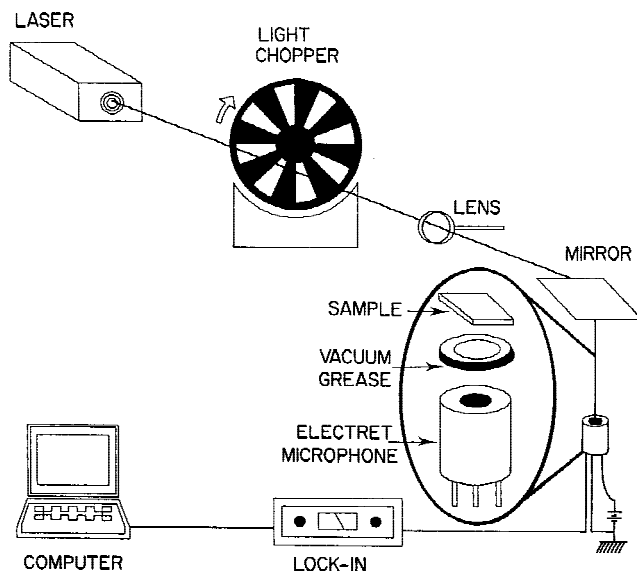


FIG. 2. Experimental setup for the employed photoacoustic technique in order to measure the thermal diffusivity.

modulation frequency, α is the thermal diffusivity of the sample and L its thickness. For many samples, the thermal diffusivity, α , can be obtained by means of fitting either the signal amplitude or its phase-lag using the Eqs. (1) and (2) in the range of high modulation-frequency, corresponding to a thermally thick regime ($a \gg 1$). Care should be taken when fitting, in order to avoid the frequency interval at which the noise-to-signal ratio is considerable or at which the thermoelastic effect is present.^{14,19}

In the frequency range $0 < f \leq (\pi/2)^2 f_c$, where

$$f_c = \frac{a}{L^2 \pi} \text{ is the cutoff frequency} \quad (3)$$

the phase Eq. (2) is approximately given by

$$\Delta\varphi = -\frac{1}{\pi f_c} f + \frac{3\pi}{4} \quad (4)$$

and the relative error in this approximation is smaller than 1.2%.²⁰ Hence, by means of fitting the experimental data of the PA signal phase using the simple linear equation [Eq. (4)] the cutoff frequency f_c can be obtained, and then, from Eq. (3) the thermal diffusivity of the sample can be deduced. This last method is most suitable for materials with high heat diffusion capacity such as metals, or some semiconductors, as well as for samples whose thickness is small. Since for these materials, the thermally thick regime can occur in hundreds or several thousands of Hz with the inconvenience that the noise-to-signal ratio becomes important and that the thermoelastic binding mechanism is present.

The heat capacity per unit volume (ρc), where ρ is the density and c is the specific heat capacity, can be determined by the thermal relaxation method²¹ with the aid of a vacuum chamber described elsewhere.²² This method is also known as the temperature-rise method under continuous light illumination. A diagram of the experimental set up is shown in Fig. 3. Both surfaces of the sample were sprayed with black paint, in order to ensure a light absorbing surface, and a constant heat transfer coefficient. The sample was then glued to the end of a thin nylon rod inside the vacuum chamber (10^{-4} torr). The optical access was through a glass window. One of the painted surfaces was then continuously and uniformly exposed to a laser beam that was expanded, and a thin thermocouple, attached to the other surface with thermal paste, was used to monitor the temperature. The temperature rise is given by

$$\Delta T = P_0 [1 - e^{-t/\tau}] / \eta \quad (5)$$

where P_0 is the incident light intensity, $\eta = 4\epsilon\sigma T_0^3$, and

$$\tau = \frac{L\rho c}{8\epsilon\sigma T_0^3} \quad (6)$$

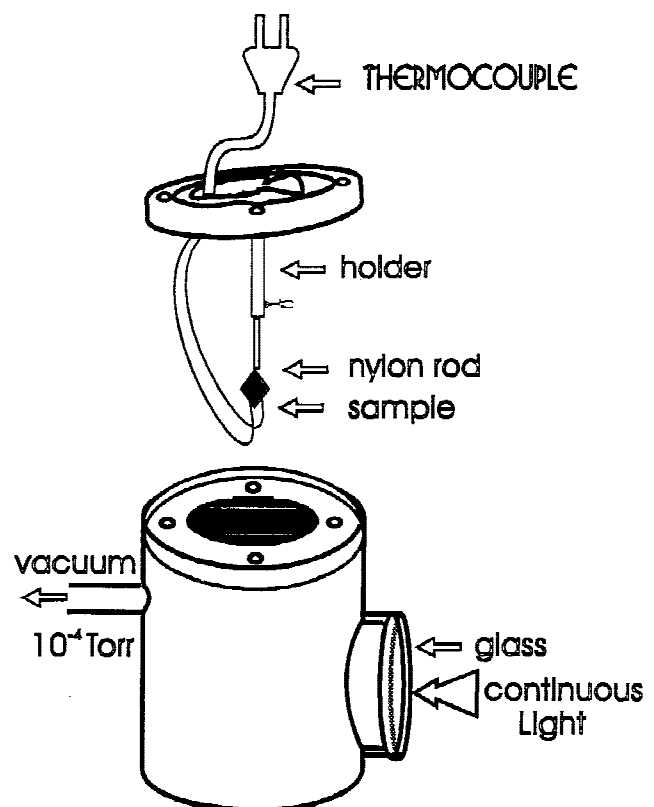


FIG. 3. The vacuum chamber for the thermal relaxation method used to determine the heat capacity per unit volume.

where $\sigma = 5.67 \times 10^{-12} \text{ W/cm}^2\text{K}^4$ is the Stefan-Boltzmann constant, ϵ is the emissivity (which is close to one), T_0 is the ambient temperature in Kelvin, and L is the sample thickness in centimeters. Equation (5) is employed with the experimental data gathered, and τ is the parameter that has to be adjusted to determine ρc . After reaching experimental saturation in temperature, described

by Eq. (5), the value of ρc can be confirmed by turning off the incident light, in which case the temperature decay will be described by

$$\Delta T = P_0 e^{-t/\tau} / \eta \quad (7)$$

and the decay relaxation time τ should be the same as that in Eq. (5).

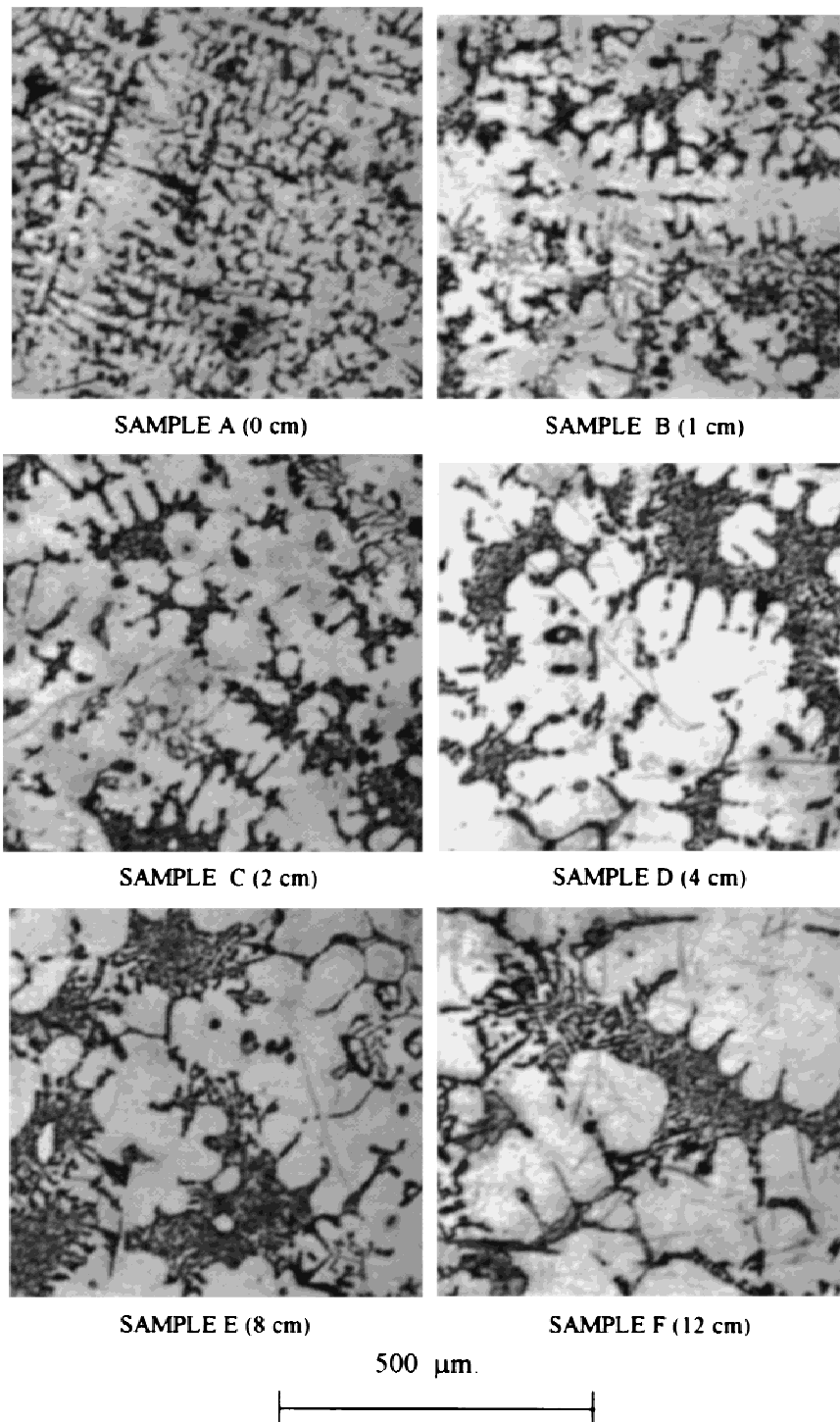


FIG. 4. Optical micrographs at different positions within the ingot.

III. RESULTS AND DISCUSSION

Typical microstructures of the samples are shown in Fig. 4, in which the dominance of the dendrites over secondary precipitates can be appreciated. The secondary dendrite arm spacing and the perimeter of dendrites were determined. These microstructural parameters are reported in Table II. Also in this table the solidification rate for each sample is reported. DAS is related to the solidification rate in Fig. 5 (solid circles), and as the rate increases, their size is reduced. The relationship found in this work is

$$\lambda = 36.1R^{-0.34}, \quad (8)$$

where λ (measured in μm) is the DAS and R is the solidification rate, which was obtained by thermal analysis of the solidification curves.²⁸ In Fig. 5 data reported

by other researchers^{23–27} are also shown. The DAS data obtained in this work are close to those reported by Granger and Ting.²⁶

Typical results of the variation of the PA phase lag as a function of the modulation frequency are shown in Fig. 6. The continuous lines are the results of least square fittings to the expression given in Eq. (4), from which the thermal diffusivities of the samples were determined, and are listed in Table II. There is a decrease of 20% in the thermal diffusivity from the bottom to 12-cm height of the ingot (Fig. 1), while the DAS increases by a factor of four. The decrease of the thermal diffusivity cannot be explained in terms of the chemical composition of the samples, in which a variation of the silicon content of 0.77% in weight occurs. More important than the amount

TABLE II. Microstructure and thermal characterization parameters.

Sample	Position in the alloy (cm)	Solidification rate (K/s)	Dendrite perimeter (mm)	Dendrite arm spacing (μm)	Heat capacity/vol ($\text{J}/\text{cm}^3\text{K}$)	Thermal diffusivity (cm^2/s)	Thermal conductivity (W/mK)
A	0	3.35	44.1	23.4	1.11	0.98	108.8
B	1	1.43	32.0	34.4	0.95	0.97	91.7
C	2	0.48	30.1	40.8	0.90	0.95	85.5
D	4	0.24	15.1	55.8	0.88	0.93	81.8
E	8	0.11	12.5	71.2	0.82	0.92	75.3
F	12	0.06	6.3	104.2	0.85	0.91	77.3

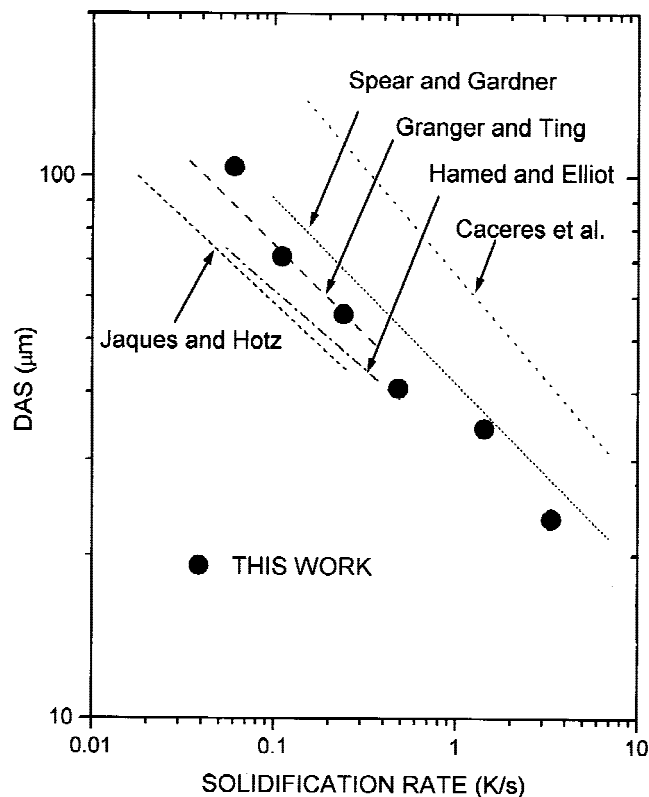


FIG. 5. Relationship between DAS and solidification rate (filled circles). Results from other researchers are included for comparison.

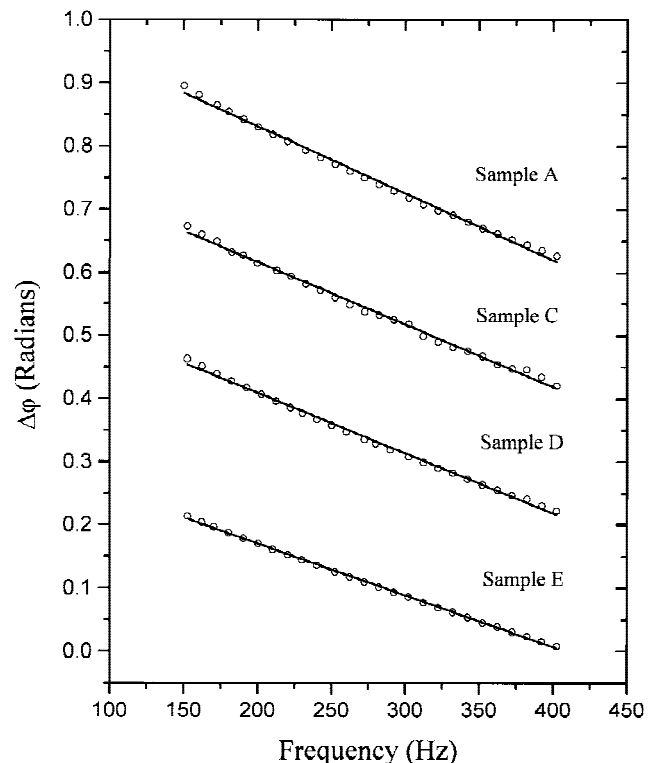


FIG. 6. Experimental results (open symbols) and fitting of Eq. (4) (continuous lines) of the PA phase lag.

of silicon is its distribution in the alloy, since Si will act as a thermal barrier.²⁹ It was found in the present study that the degree of modification was the same for all the samples. The decrease is related to the dendrite parameter DAS, which determines the form of the aluminum channels. Since the thermal diffusivity measures essentially the thermalization time within the sample (the greater the thermal diffusivity, the less the heating time), a greater thermal diffusivity is expected near the bottom of the ingot, where the DAS is finest.

Figure 7 shows a typical result of thermal relaxation experiments. The solid lines correspond to the best fits of Eq. (5) (increasing temperature) and Eq. (7) (decreasing temperature) to the experimental data, from which the value of ρc is deduced, Table II.

The dependence of the thermal conductivity, $k = \alpha\rho c$, on the DAS is shown in Fig. 8. The behavior corresponds to an allometric function of the form:

$$k = 230\lambda^{-0.253} \quad (9)$$

The dependence of the conductivity on the dendrite perimeter is shown in Fig. 9. The variation in the thermal conductivity as a function of the dendrite perimeter follows a linear trend.

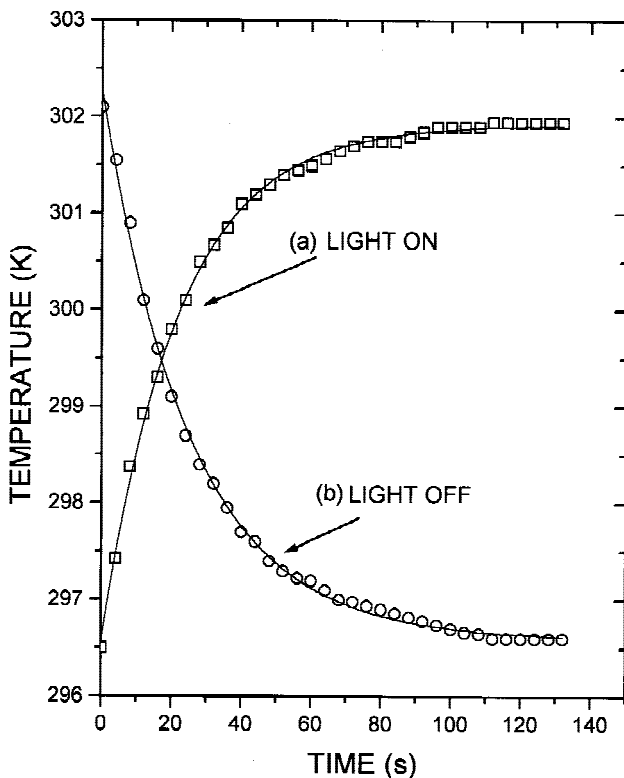


FIG. 7. (a) Experimental increase of temperature and fitting of Eq. (5) (continuous curve) under continuous illumination. (b) Decrease of temperature after turning off the light, with fitting of Eq. (7) (continuous line).

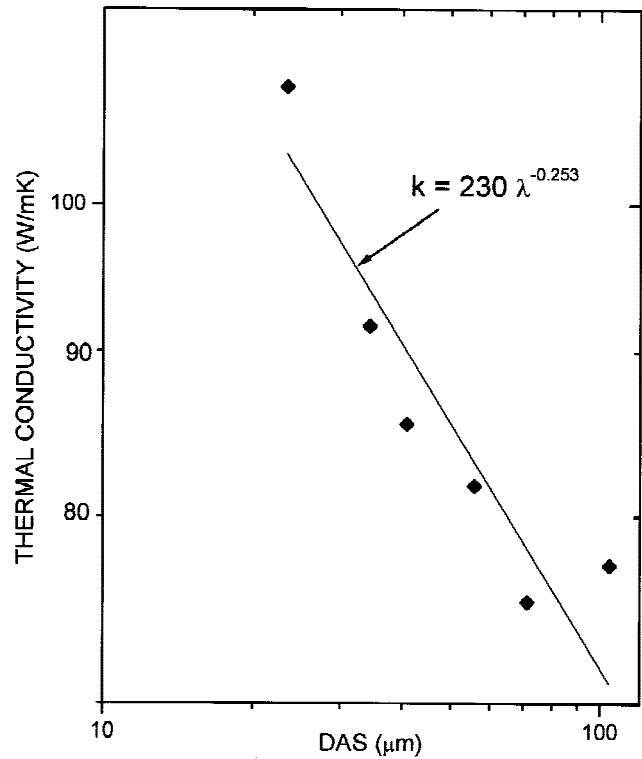


FIG. 8. Variation in thermal conductivity as a function of secondary dendrite arm spacing.

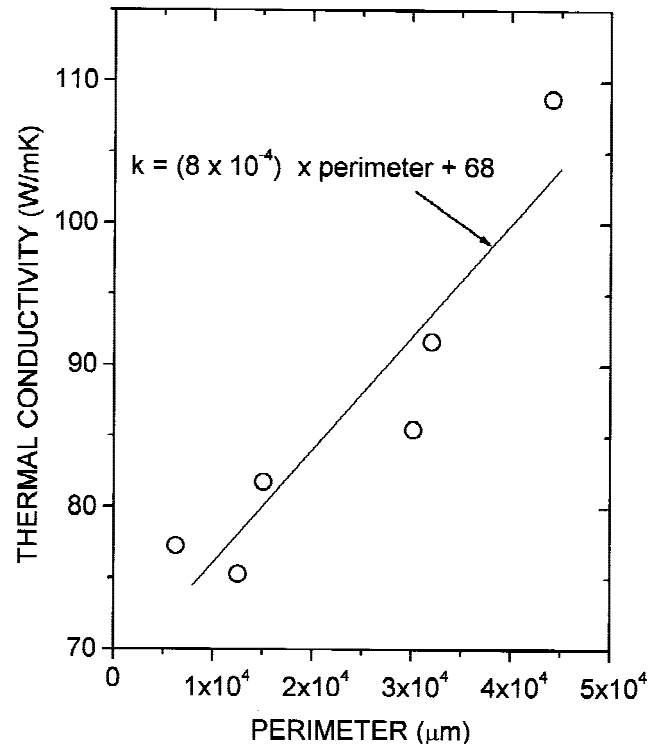


FIG. 9. Variation in thermal conductivity as a function of dendrite perimeter.

These results indicate that the thermal conductivity is increased when the microstructure is refined, which means that an adequate design in terms of mechanical properties, will also enhance the thermophysical ones, which will benefit the resistance to thermal fatigue.³⁰

IV. CONCLUSIONS

The thermophysical properties of a series of samples of an aluminum casting alloy were determined as a function of the principal microstructural parameters, namely the secondary dendrite arm spacing and the integral dendrite perimeter. The measurements were performed using the photoacoustic effect and the thermal relaxation method. It was found that the effective thermal conductivity increases linearly with the dendrite perimeter.

ACKNOWLEDGMENTS

This work was partially supported by Consejo Nacional de Ciencia y Tecnología (CONACyT), México. The authors would like to thank Eng. Blanca Zendejas for her valuable technical support. The support of Corporativo Nemak S.A. de C.V. is also acknowledged.

REFERENCES

1. P.M. Norris, M.C. Hastings, and W.J. Wepfer, *J. Exp. Heat. Trans.* **7**, 43 (1994).
2. J.A. Horwath and L.F. Mondolfo, *Acta Metall.* **10**, 1037 (1962).
3. M.C. Flemings, T.Z. Kattamis, and B.P. Bardes, *AFS Trans.* **88**, 695 (1980).
4. R.M. Kotschi and C.R. Loper, Jr., *AFS Trans.* **85**, 425 (1977).
5. J. Campbell, *Castings* (Butterworth-Heinemann, London, 1991).
6. I.J. Polmear, *Light Alloys* (Arnold, a division of Hodder Headline PLC, London, 1996).
7. J.L. Carbajal, C. Casado, J.F. Mojica, and S. Valtierra, 3rd. Int. Conf. Molten Aluminum Processing (AFS, Des Plaines, IL, 1992), p. 141.
8. L. Mondolfo, *Aluminum Alloys, Structure and Properties* (Butterworth, London, 1986).
9. L. Backerud and E. Krol, *Solidification Characteristics of Aluminum Alloys* (Foundry Alloys, Skan Aluminum, Oslo, 1990), Vol. 2.
10. J.E. Hatch, *Aluminum Properties and Physical Metallurgy* (ASM, Metals Park, OH, 1984).
11. P.K. Kuo, L. Wei, and R.L. Thomas in *Photoacoustic and Photothermal Phenomena III*, Springer Series in Optical Sciences Vol. 69, edited by Theodor Tamir (Springer-Verlag, Berlin, 1992).
12. E. Feit and H. Shaw, *Am. Ceram. Soc. Bull.* **70**, 125 (1991).
13. A.J. Ångstrom, *Phil. Mag.* **26**, 130 (1863).
14. L.F. Perondi and L.C.M. Miranda, *J. Appl. Phys.* **62**, 2955 (1987).
15. M.E. Rodríguez, J. M. Yáñez, A. Cruz, J.J. Alvarado, O. Zelaya, F. Sánchez, H. Vargas, J.D. Figueroa, F. Martínez, J. Martínez, J. González, and L.C.M. Miranda, *Z. Lebensm, Unters Forsch.* **201**, 236 (1995).
16. M. Yáñez, M.E. Rodríguez, J.J. Alvarado, O. Zelaya, F. Sánchez, A. Cruz, H. Vargas, J.D.C. Figueroa, F. Martínez, J. Martínez, J. González, C. Argüello, and L.C.M. Miranda, *Analyst bf.* **120**, 1953 (1995).
17. A. Calderón, J.J. Alvarado Gil, Y. Gurevich, A. Cruz Orea, I. Delgadillo, H. Vargas, and L.C.M. Miranda, *Phys. Rev. Lett.* **79**, 5022 (1997).
18. A. Cruz-Orea, I. Delgadillo, H. Vargas, A. Gudiño, E. Marin, C. Vázquez-López, A. Calderón, and J.J. Alvarado, *J. Appl. Phys.* **79**, 8951 (1996).
19. G. Rousset, F. Lepoutre, and L. Bertrand *J. Appl. Phys.* **54**, 2383 (1983).
20. A. Calderón, R.A. Muñoz Hernández, S.A. Tomás, A. Cruz Orea, and F. Sánchez Sinencio, *J. Appl. Phys.* **84**, 6327 (1998).
21. I. Hatta, *Rev. Sci. Inst.* **50**, 292 (1979).
22. G. Gutiérrez-Juárez, O. Zelaya, Juan J. Alvarado-Gil, H. Vargas, H. de O. Pastore, J.S. Barone, M. Hernández, and L. Baños, *J. Chem. Soc., Faraday Trans.* **92**, 2651 (1996).
23. C.H. Caceres, C.J. Davidson, and J.R. Griffiths, *Mater. Sci. Eng.* **A197**, 171 (1995).
24. R.E. Spear and G.R. Gardner, *Trans. AFS.* **71**, 209 (1963).
25. Q.S. Hamed and R. Elliot, *Cast Metals.* **6**, 36 (1993).
26. D.A. Granger and E. Ting, in *Structures in Directionally Solidified Aluminum Foundry Alloy*, edited by D.M. Stefanescu, G.J. Abbaschian, and R.J. Bayuzick (The Metallurgical Society, London, United Kingdom, 1988), p. A356.
27. J.C. Jaques and W. Hotz, *Cast Metals.* **4**, 200 (1992).
28. E. Velasco, F. Hernandez, J.G. de la Rosa, S. Valtierra, J.F. Mojica, and R. Colas in *Light Metals*, edited by B. Welch (TMS, Warrendale, PA, 1998) p. 993.
29. J.E. Gruzleski and B.M. Closset, *The Treatment of Liquid Aluminum-Silicon Alloys* (AFS, Des Plaines, 1990).
30. R.B. Gundlach, *Thermal Fatigue Resistance of Aluminum Alloy 319* (Climax Research Services, Cleveland, OH, 1993).